European Journal of Nuclear Medicine and Molecular Imaging
https://doi.org/10.1007/s00259-020-05183-1

ORIGINAL ARTICLE

Indication of retrograde tau spreading along Braak stages and functional connectivity pathways

Joseph Seemiller[1] · Gérard N. Bischof[2] · Merle C. Hoenig[2,3] · Masoud Tahmasian[4] · Thilo van Eimeren[2,5,6] · Alexander Drzezga[2,3,6] · and the Alzheimer's Disease Neuroimaging Initiative

Received: 7 September 2020 / Accepted: 27 December 2020

Abstract

Purpose Tau pathology progression in Alzheimer's disease (AD) is explained through the network degeneration hypothesis and the neuropathological Braak stages; however, the compatibility of these models remains unclear.

Methods We utilized [18F]AV-1451 tau-PET scans of 39 subjects with AD and 39 sex-matched amyloid-negative healthy controls (HC) in the ADNI (Alzheimer's Disease Neuroimaging Initiative) dataset. The peak cluster of tau-tracer uptake was identified in each Braak stage of neuropathological tau deposition and used to create a seed-based functional connectivity network (FCN) using 198 HC subjects, to identify healthy networks unaffected by neurodegeneration.

Results Voxel-wise tau deposition was both significantly higher inside relative to outside FCNs and correlated significantly and positively with levels of healthy functional connectivity. Within many isolated Braak stages and regions, the correlation between tau and intrinsic functional connectivity was significantly stronger than it was across the whole brain. In this way, each peak cluster of tau was related to multiple Braak stages traditionally associated with both earlier and later stages of disease.

Conclusion We show specificity of healthy FCN topography for AD-pathological tau as well as positive voxel-by-voxel correlations between pathological tau and healthy functional connectivity. We propose a model of "up- and downstream" functional tau progression, suggesting that tau pathology evolves along functional connectivity networks not only "downstream" (i.e., along the expected sequence of the established Braak stages) but also in part "upstream" or "retrograde" (i.e., against the expected sequence of the established Braak stages), with pathology in earlier Braak stages intensified by its functional relationship to later disease stages.

Keywords Alzheimer's disease · Tau · PET · Functional connectivity · Braak stage · Network degeneration hypothesis

This article is part of the Topical Collection on Neurology – Dementia

✉ Joseph Seemiller
joe@josephseemiller.com

Gérard N. Bischof
gerard.bischof@uk-koeln.de

Merle C. Hoenig
merle.hoenig@uk-koeln.de

Masoud Tahmasian
masoudtahmasian@gmail.com

Thilo van Eimeren
thilo.van-eimeren@uk-koeln.de

Alexander Drzezga
Alexander.Drzezga@uk-koeln.de

[1] Department of Neurology, Geisinger Medical Center, 100 N. Academy Ave, Danville, PA 17822, USA

[2] Multimodal Neuroimaging Group, Department of Nuclear Medicine, Faculty of Medicine and University Hospital Cologne, University of Cologne, 50937 Cologne, Germany

[3] Molecular Organization of the Brain, Institute of Neuroscience and Medicine 2, Research Center Juelich, Jülich 52428, Germany

[4] Institute of Medical Science and Technology, Shahid Beheshti University, Tehran, Iran

[5] Department of Neurology, Faculty of Medicine and University Hospital Cologne, University of Cologne, 50937 Cologne, Germany

[6] German Center for Neurodegenerative Diseases (DZNE), Bonn/ Cologne, Germany

Published online: 18 January 2021

Introduction

Misfolded proteins have been found to aggregate within specific vulnerable brain regions [1] and progress to other brain regions that are often anatomically connected [2]. The network degeneration hypothesis (NDH) proposes that neurodegenerative diseases, including Alzheimer's disease (AD), target large-scale brain networks [3] and their pathology follows functional connectivity (FC) patterns [4–7].

The topographical distribution of tau corresponds with several higher order cognitive networks [8], suggesting that tau progresses from more than one pathologic epicenter [9, 10] and progresses system-wide rather than focally [11], and that ROI-based intrinsic functional connectivity (iFC) covaries with tau [4]. The sentinel stagewise neuropathological tau progression model suggested by Braak and Braak suggests that tau aggregation begins in the entorhinal cortex and locus coeruleus [12], with subsequent accumulation of tau in the mesocortex, allocortex, and then neocortex. The extent of stagewise tau pathology implies a progression of protein from earlier to later stages ("anterograde progression"). However, multiple in vitro studies [13] and in vivo studies [14, 15] have suggested that tau could, at least in part, propagate in reverse ("retrograde progression"). The mis-sorting hypothesis, contending that tau is not sorted into axons but rather accumulates in the somatodendritic compartment of neurons [16], could help to account for retrograde progression. Furthermore, progression of tau pathology has been related to synaptic connectivity rather than spatial proximity, both along efferent and afferent connections [14], and this finding has been replicated in vivo by tau-PET imaging studies [17–19]. The compatibility of the stagewise progression of tau according to Braak and Braak with the NDH, especially with the possibility of both anterograde and retrograde progressions of tau, has not been sufficiently explored. Although the sentinel stagewise neuropathological tau progression model suggested by Braak and Braak [12] has been replicated in vivo by tau-PET imaging studies [17–19], its relationship with the NDH has not been well explored.

We hypothesized that tau pathology advances progressively based on the iFC of already affected regions, consistent with the multiple resting state functional connectivity networks (rs-FCNs) related with tau pathology found in other studies [8, 10]. As each new hub, or peak region of tau-tracer retention (tau-peak), is afflicted with tau, it contributes uniquely to tau's future progression within other unique brain regions.

We employed a novel approach to study the relationship between the NDH and Braak stages, using [18F]AV-1451 tau-PET imaging and resting state fMRI (rs-fMRI). We identified tau-peaks, which we hypothesized to represent major epicenters of functionally related tau progression across the brain. Each tau-peak was used as a seed to generate a corresponding healthy FCN using healthy control (HC) subjects. We examined the relationship between pathological tau deposition levels (AD > HC) and functional connectivity (in HC) within the respective seed-based FCNs, both within all areas of significant tau deposition and, then again, restricted to individual Braak stage-maps and their component AAL ROIs. Our analysis uniquely comments on the relationship between tau and functional connectivity levels within individual Braak stages. With this data, we suggest that the extent of AD-pathological tau is consistent with the Braak stages and the network degeneration hypothesis.

Materials and methods

Data

Data used in the preparation of this article were obtained from the Alzheimer's Disease Neuroimaging Initiative (ADNI) database (adni.loni.usc.edu). The ADNI was launched in 2003 as a public-private partnership, led by Principal Investigator Michael W. Weiner, MD. The primary goal of ADNI has been to test whether serial magnetic resonance imaging (MRI), positron emission tomography (PET), other biological markers, and clinical and neuropsychological assessment can be combined to measure the progression of mild cognitive impairment (MCI) and early Alzheimer's disease (AD). For up-to-date information, see www.adni-info.org.

Subjects

This study included all available subjects with a clinical, non-biomarker-defined diagnosis of AD and with available AV-1451 PET and T1-weighted MRI imaging at the time of project initiation (November 2019); a matching number of randomly selected amyloid-negative HC subjects were included and were sex-matched to the AD subjects. Amyloid negativity was defined, as described on the ADNI website, as having a standardized uptake value ratio (SUVr) of less than 1.11 using the Florbetapir tracer or less than 1.08 using the Florbetaben tracer. In total, 39 subjects with AD and 39 subjects with HC were included in the study. A summary of demographic characteristics is reported in Table 1.

MRI acquisition

T1-weighted MR scans were used in this study which were generated according to the ADNI acquisition protocol [20]. Baseline images of subjects were used in this study, and the screening image was used if the baseline was unavailable.

Table 1 Demographic information about the datasets used

Group	Age	Education	MMSE	CDR-SB	Males	Females
AD patient ($N = 39$)	73.9 ± 8.7	15.9 ± 2.4	22.8 ± 2.7	4.4 ± 1.6	26	13
HC($N = 39$)	69.6 ± 5.2	16.9 ± 2.1	29.2 ± 1.0	0.1 ± 0.1	26	13
HC (fMRI only)* ($N = 198$)	21.0 ± 2.3				75	123

*From the functional connectome project

CDR-SB, clinical dementia rating–sum of boxes; MMSE, mini-mental state examination

PET acquisition

AV1451 imaging was performed according to ADNI acquisition protocol. Images were taken over 30 min, in six 5-min frames, starting 75 min after 10 mCi of F-AV-1451 injection. Images taken from ADNI were already coregistered and averaged.

Voxel-wise data processing

Using Statistical Parametric Mapping (SPM) version 12 (Wellcome Trust Centre for Neuroimaging, Institute of Neurology, University College London), each subject's PET scan was coregistered to its corresponding T1 MRI scan. Coregistered MRI images were segmented and normalized to Montreal Neurological Institute (MNI) space. Partial volume correction was performed using PETPVE12 toolbox [21]. SUVR images were calculated using the inferior cerebellar grey matter as a reference. Inferior cerebellar grey matter was obtained from the SUIT template [22] and transformed into each subject's native space, similar to published methods [23]. Finally, the normalization deformation of the MRI into MNI space was also applied to the corresponding PET image and images were smoothed to 10 × 10 × 10 mm.

Braak stages

Maps of Braak stages 1–6 (Braak stage-maps, or BR1–6) were established as indicated in Table 2. BR1–2 consisted of the entorhinal cortex as defined in the Juelich histological atlas [24]. Specific ROIs from the automated anatomical labeling (AAL) atlas (Table 2) were used to create BR3–6, similar to a previously described ROI-based Braak staging approach [10, 19, 25].

Voxel-wise PET data analysis

A voxel-wise group comparison of tau-PET images was performed between AD and HC subjects ($p < 0.05$, without FWE correction), controlling for age as a covariate. This spatial distribution map was z-score-transformed and mean values were taken within each Braak stage-map (Table 2). Next, the voxel with the highest t score (tau-peak, $p < 0.05$) was identified within each individual Braak stage. Tau-peaks were subsequently employed in a seed-based functional connectivity analysis.

FMRI data acquisition and preprocessing

rs-fMRI analyses were performed using publicly available imaging data from the 1000 Functional Connectomes Project (FCP) [26]. One hundred ninety-eight rs-fMRI images from the Cambridge-Buckner dataset of the FCP aged 18–30 were used (Table 1). FC analysis was performed using SPM and the Data Processing Assistant for Resting-State fMRI (DPARSF) version 4.0, a pipeline analysis toolbox.

Preprocessing steps followed the standard protocol [27]. For acquisition of rs-fMRI data, participants in this dataset were instructed to rest while remaining awake with eyes open in a 3-T scanner. rs-fMRI data was acquired using an echo-

Table 2 Braak stage components and mean pathological tau. For each Braak stage in the first column, its respective definition based on automated anatomical labeling (AAL) regions of interest, as well as the mean voxel-wise Z-score (AD > HC, $p < 0.05$ without FWE correction)

Braak stage	ROIs	Mean Z-score in AD > HC
I/II	Entorhinal cortex (in Jülich Histological Atlas)	2.36
III	AAL ROIs: parahippocampal gyrus, fusiform gyrus, lingual gyrus, amygdala	2.81
IV	AAL ROIs: inferior temporal cortex, middle temporal cortex, temporal pole, thalamus, posterior cingulate, insula	3.35
V	AAL ROIs: frontal cortex, parietal cortex, occipital cortex, superior temporal cortex, precuneus, caudate nucleus, putamen	3.01
VI	AAL ROIs: precentral gyrus, postcentral gyrus, paracentral gyrus, cuneus	2.67

planar imaging (EPI) sequence, with a repeat time (TR) = 2 s, echo time (TE) = 30 ms, time points = 119, slice number = 47, voxel size = 3 × 3 × 3 mm^3, and field of view = 216 × 216. A high-resolution T1-weighted magnetization-prepared gradient echo (MPRAGE) image was also obtained for each subject in order to spatially normalize the rs-fMRI scans.

To avoid transient changes before reaching a steady state, the first ten time points of each subject were discarded, and then, scans were processed with slice timing. Nuisance variables were regressed from the fMRI signal including white matter and CSF signal. Global signal regression was also performed, which has been shown to be very effective at removing artifact [28] despite debate [29–31] and physiological noise, including respiratory and cardiac-based signals. Next, head motion was corrected using the Friston 24 parameter model [32], as higher parameter confound regression models are suggested to be beneficial in removing motion [28]. Then, a T1-weighted normalization of the fMRI scans was performed into MNI space, followed with band-pass filtering (0.01–0.1 Hz), and smoothed with a 4 mm × 4 mm × 4-mm Gaussian kernel to reduce spatial noise.

Rs-fMRI analysis

Separately, at each tau-peak, a seed in the form of a sphere of 4-mm radius was positioned. Seed-based FC analyses for each respective tau-peak were performed on the 198 rs-fMRI HC subjects, controlling for age and sex to identify characteristic intrinsic networks ($p < 0.05$, without FWE correction).

t test and GOF comparison of tau and iFC

A goodness of fit (GOF) analysis compared the average *t* scores, and a *t* test assessed for significance between tau (AD > HC, $p < 0.05$, without FWE correction) inside versus outside of each FCN (HC, $p < 0.05$, without FWE correction). GOF scores were calculated as average tau *t* scores inside the FCN divided by that outside of the FCN.

Correlation between tau and iFC

Voxel-wise spearman correlation analyses were performed between the *t* score map of the tau-tracer retention pattern (AD > HC, $p < 0.05$, without FWE correction) and the *t* score maps of the generated tau-peak FCNs ($p < 0.05$, without FWE correction), respectively. *t* scores of the tau-peak FCNs represent the iFC to the respective tau-peak. A sphere of 10-mm radius surrounding each tau-peak was removed from the correlation analysis in order to eliminate interference from voxels near the tau-peak tending to have a higher level of functional connectivity. All *t* tests and correlations were performed both across all significant tau voxels and, again, restricted to significant voxels in each Braak stage-map and again in each individual Braak stage-map AAL region.

All *p* values were corrected for multiple comparisons using FDR-correction in MATLAB, correcting for all permutations (125) of FCNs with Braak stages and Braak stage-maps. The strength of the correlation between tau and iFC in each Braak stage was compared to the correlation strength in its stage-map AAL regions using the Fisher *Z*-test from the Cocor package [33]. In each ROI, if an FCN had a significantly greater burden of tau inside relative to outside the FCN, and the correlation between tau and iFC in that FCN was significantly stronger than across the whole brain, then that FCN was thought to be implicated in the progression of tau within that ROI.

Results

Patterns of tau-tracer retention

The group-level comparison *t* test between the tau-tracer retention of AD and HC groups revealed a pattern of increased tau-tracer retention in AD as compared to HC, including the posterior cingulate cortex, precuneus, inferior temporal, occipital, and frontal cortical region. The mean *z*-score in AD > HC subjects (Table 2, $p < 0.05$, without FWE correction) within each Braak stage (Fig. 1) showed the highest AD-pathological tau in BR4 with mean levels subsequently declining in stages BR5–6.

Locations of tau-peaks

Five tau-peaks were determined, one for each Braak stage, and were named after their corresponding stage (i.e., tau-peak 3 was the peak of Braak stage 3). Tau-peak 1–2 was in the right entorhinal cortex, tau-peak 3 in the left fusiform gyrus, tau-peak 4 in the left middle temporal lobe, tau-peak 5 in the left parietooccipital junction, and tau-peak 6 in the left cuneus. Visualizations of tau-peaks (Fig. 1) and FCNs (Figs. 1 and 2) are provided.

FCNs correspond to greater burden of tau pathology

There was significantly more tau pathology falling within relative to outside of FCNs. GOF ratios, comparing average tau deposition (AD > HC, $p < 0.05$) inside of an FCN (HC, $p < 0.05$) relative to that outside of an FCN. This relationship was preserved and often stronger within specific Braak stages or AAL regions of the Braak stages. For example, GOF ratios ranged from 1.06 to 1.17 across the whole brain, and as high as 1.41 in the cingulum, inside compared to outside of FCN 6 (Table 3).

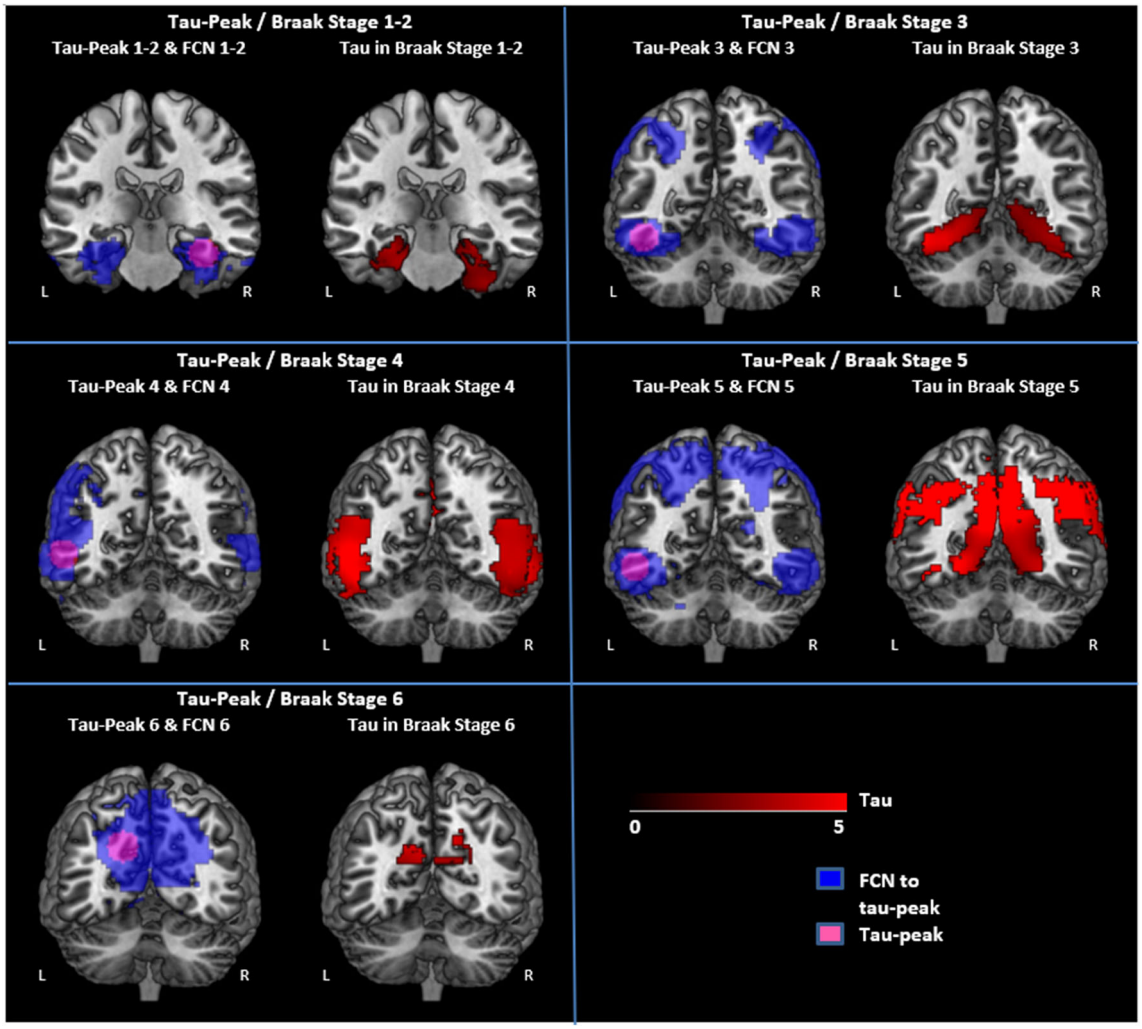

Fig. 1 Tau-peaks and their associated FCNs. Tau-peaks 1–6 (pink) are visualized as 1.0-cm spheres with their respective FCN (blue). The extent of significant tau (AD > HC, $p < 0.05$, without FWE correction) in each Braak stage is shown in red. Each tau-peak is named after the Braak stage of which it is the peak value (i.e., tau-peak 1–2 is the peak of Braak stage 1–2). FCN (functional connectivity network)

Voxel-wise tau deposition correlates with iFC to each tau-peak

t scores of voxel-wise pathological tau deposition (AD > HC, $p < 0.05$) correlated positively with each voxel's respective iFC *t* score (HC, $p < 0.05$) within the FCN of tau-peaks 1–5 (Table 3). The relationship between iFC and tau was re-analyzed within each individual Braak stage, as well as within each individual AAL region of every Braak stage. In many cases, these relationships between pathological tau deposition and iFC were significantly stronger ($p < 0.05$, Table 3) within whole Braak stage-maps, or within AAL regions of the Braak stages, than they were across the whole brain.

Significant correlations ($p < 0.01$) were observed between iFC levels of voxels to a tau-peak and levels of tau deposition, in those same voxels, both within earlier Braak stages ("backward/upstream" relationships) and more advanced Braak stages ("forward/downstream" relationships), as shown in Fig 3. For example, tau-peak 4 had iFC that correlated significantly with tau deposition within BR3 ("upstream") and within BR5 ("downstream").

Discussion

Summary

This study is the first to assess the tau-iFC relationship both regarding the voxel-wise topographical overlap of iFC with tau and with a voxel-wise correlation between iFC and tau. Furthermore, the tau-iFC relationship is significantly stronger in specific Braak stage-maps both more and less advanced than the respective tau-peak. We found that the peak clusters of tau deposition (tau-peaks) have patterns of iFC (in HC subjects) with a topography that is specific for tau in specific regions, represented in high goodness of fit ratios and

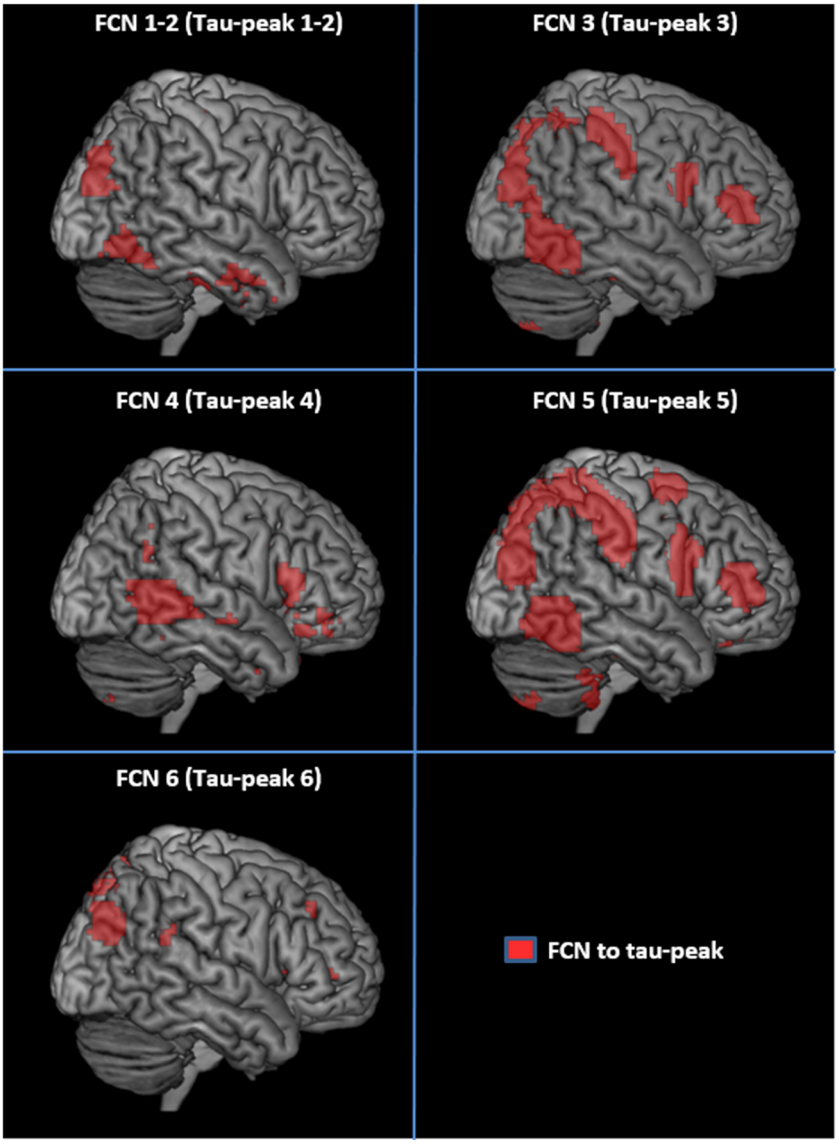

Fig. 2 FCN surface projections. FCNs 1–6 (red) visualized as surface projections. The tau-peak from which each respective FCN was derived is listed in parenthesis, and its number refers to the tau-peak's corresponding Braak stage. The right hemisphere was chosen for illustration purposes given the bilateral activation of FCNs. FCN (functional connectivity network)

consistent with *t* tests. Furthermore, iFC correlates positively with levels of tau-tracer deposition (AD > HC) in the same respective voxels, and significantly moreso in specific regions of the brain. These relationships support our proposal of an anterograde and retrograde, or downstream and upstream, pattern of tau pathology progression.

Tau deposition pattern

We observed a pattern of significant tau-tracer retention in patients with AD compared to HC subjects in the posterior cingulate cortex, precuneus, inferior temporal, occipital, and frontal regions. This pattern complies with the expected pattern of neurofibrillary tangle pathology as known from neuropathological studies [12] and studies using in vivo tau-PET imaging in AD [17, 18, 34].

Levels of tau deposition

The extent of pathological tau deposition, lowest in stage BR1–2, might initially appear contradictory to studies postulating the onset of tau aggregation to be in the mesial temporal lobes [12]. However, significant tau-tracer retention can be observed in the hippocampus and entorhinal cortex of the non-demented elderly [35–37], thus reducing the relative difference of tracer uptake in these regions in AD versus HC.

Regional tau deposition represents disease chronology

We hypothesized that regional tau-tracer retention would indirectly reflect the chronological order of disease expansion, assuming that regions affected early in the disease accumulated a relatively higher pathological tau burden as compared to

Table 3 Comparison of tau deposition with FCNs. Two-tailed *t* tests and goodness of fit ratios were used to compare the level of tau deposition (AD > HC, $p < 0.05$) within each FCN to that outside of each FCN (HC, unpaired *t* test, $p < 0.05$), within each ROI. Voxel-wise spearman correlations were computed between tau deposition (AD > HC, $p < 0.05$) and iFC (HC, unpaired *t* test, $p < 0.05$). All listed Braak stage-maps and AAL regions met both criteria of having (1) significantly more ($p < 0.05$) tau inside relative to outside the FCN and (2) a Spearman correlation between tau and iFC that is significantly stronger ($p < 0.05$) than across all tau deposition. The component AAL region with the strongest correlation is listed in brackets if meeting the criteria and if having a correlation stronger than the full Braak stage. If a full Braak stage-map did not meet the criteria, then a component AAL region is listed if meeting criteria. All *p* values are FDR-corrected for multiple comparisons.

	t test		Spearman correlation
	Braak stage/substage	GOF ratio	iFC and tau
ROI1–2 iFC	All tau	1.06	0.05; $p < 0.01$
	BR1–2	1.22	0.65; $p < 0.01$
	BR3	1.22	0.38; $p < 0.01$
	Cingulum (BR4)	1.32	0.49; $p < 0.01$
	BR5 (occipital cortex)	1.07 [1.19]	0.13; $p < 0.01$ [0.29; $p < 0.01$]
	BR6 (postcentral gyrus)	1.01 [1.05]	0.33; $p < 0.01$ [0.42; $p < 0.01$]
ROI3 iFC	All tau	1.08	0.29; $p < 0.01$
	BR1–2	1.12	0.51; $p < 0.01$
	BR3	1.22	0.50; $p < 0.01$
	BR5 (occipital cortex)	1.10 [1.21]	0.34; $p < 0.01$ [0.53; $p < 0.01$]
	BR6 (postcentral gyrus)	1.05 [1.15]	0.34; $p < 0.01$ [0.45; $p < 0.01$]
ROI4 iFC	All tau	1.17	0.38; $p < 0.01$
	BR4	1.27	0.41; $p < 0.01$
	Superior temporal cortex (BR5)	1.12	0.44; $p < 0.01$
	BR6 (precentral gyrus)	1.08 [1.19]	0.50; $p < 0.01$ [0.58; $p < 0.01$]
ROI5 iFC	All tau	1.09	0.32; $p < 0.01$
	BR3	1.20	0.61; $p < 0.01$
	BR5 (occipital cortex)	1.13 [1.26]	0.33; $p < 0.01$ [0.57; $p < 0.01$]
	BR6 (postcentral gyrus)	1.07 [1.16]	0.35; $p < 0.01$ [0.63; $p < 0.01$]
ROI6 iFC	All tau	1.06	0.22; $p < 0.01$
	Cingulum (BR4)	1.41	0.66; $p < 0.01$
	Superior temporal cortex (BR5)	1.16	0.50; $p < 0.01$
	BR6 (cuneus)	1.11 [1.17]	0.43; $p < 0.01$ [0.80; $p < 0.01$]

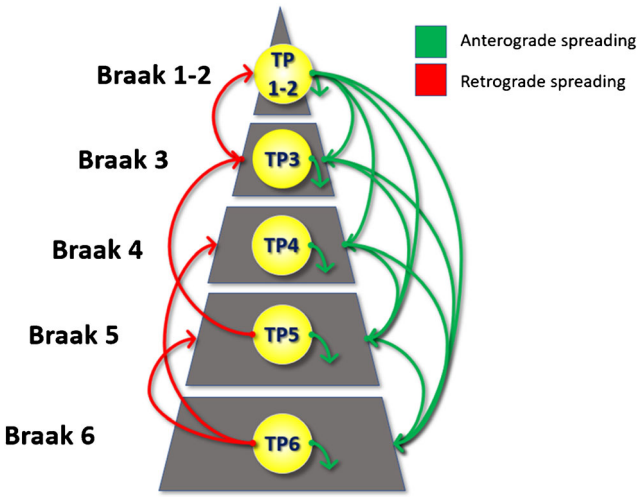

Fig. 3 Upstream and downstream patterns of Braak stagewise tau progression based on correlations between tau-peak iFC and tau deposition. Arrows originating from each tau-peak and terminating in the Braak stage in which that respective tau-peak iFC significantly correlates with tau deposition, and this relationship is significantly more positive ($p < 0.05$) within the specific Braak stage than in the entire distribution of significant tau (refer to measures of relationship strength in Table 3)

regions affected later in time, similar to hypotheses for amyloid [38]. We found that AD-pathological tau was greater in Braak stage 3–4 than in stage 5–6, reflected by average *t* scores (AD > HC, Table 2) of 3.08 across stages 3–4 and 2.84 across stages 5–6 This supports increased AD-related tau pathology present in lower Braak stages.

We suggest that AD-type tau pathology could initiate from tau-peak 1–2, in the entorhinal cortex, with further disease pathology concentrated in functionally connected regions, in both anterograde and retrograde directions.

Mechanisms of tau progression

The mechanism of tau progression has been explained by the hypotheses of (1) trans-neuronal, prion-like spread, and by (2) deposition in areas of selective vulnerability. The prion-like spreading hypothesis [39, 40] contends that tau is passed from highly connected regions or seeds [41], thus more closely matching patterns of functional activity [8, 42], but independently of any large-scale functional network [9]. Alternatively, it has been proposed that tau can accumulate in regions that are selectively vulnerable due to higher local

metabolic demand [43, 44] or lack of local neurotrophic hormones [45].

Prion-like tau spreading was supported by transgenic mouse models, in which synthetic tau fibrils induced tau aggregations and initiated tau spreading [46], spreading by synaptic connectivity rather than just spatial proximity [14]. In human models, prion-like tau spreading was found to affect intrinsic functional networks with associated behavioral dysfunction in cognitive tasks such as object recognition [47]. Together, these findings have fueled the idea that tau pathology is transmitted in a "prion-like" fashion from cell-to-cell [39], which suggests that tau may progress along actively communicating brain regions.

Structural and functional progression of tau pathology

The results of this study are compatible with both the prion-like and selective vulnerability theories of tau spreading. Genetic susceptibility for neurodegeneration could explain the specific vulnerability of tau-peaks, and their functionally connected regions, to tau deposition. The mis-sorting hypothesis, contending that tau accumulates in the somatodendritic compartment of neurons rather than being sorted to axons [16], could support retrograde progression of tau pathology within our study's proposal of bidirectional tau progression through the reversal of tau's flow.

We found that stronger regional functional connectivity to each identified tau-peak is associated with higher tau burden, on a voxel-wise basis. Regions of the brain that had a significantly stronger correlation between tau and iFC than across the whole brain also re-demonstrated topographical specificity for tau, as represented in the GOF. These results are consistent with studies suggesting that functional hubs are particularly susceptible to tau based on their weighted degree or connectivity [9, 48], and that higher functional connectivity between two ROIs is associated with greater covariance of tau levels between those two ROIs [4].

Patterns of tau accumulation

Despite most cases of AD conforming to the typical Braak staging pattern [17–19, 49], there are many noted cases of interindividual heterogeneity [50–53], including different clinical profiles such as logopenic primary progressive aphasia and posterior cortical atrophy. While our study does not account for multiple distinct phenotypes of tau progression, a recent preprint that identified four specific patterns of tau progression also noted overlap of the phenotypes in early stages of dementia [54]. With a mean MMSE of 22.8 and CDR-SB of 4.4, our AD population had a milder clinical level of dementia, which could lessen the extent of phenotypic differences in tau pathology patterns through our subjects.

Interindividual differences were accounted for in a recent study [48] that identified epicenters of tau within each individual's tau-PET scans. Cross-sectionally, tau deposition was related to iFC strength to the tau epicenters, and longitudinally, tau accumulated in regions most strongly connected to the tau epicenter. In contrast, our study found epicenters on a group-wise basis and correlations on a voxel-wise basis, finding a similar cross-sectional relationship between iFC and tau; additionally, our analysis quantifies the topographical similarity of tau and iFC using goodness of fit.

Our study looked at overall AD-pathological tau without specificity for multiple subtypes or interindividual differences. Our conclusion is in support of the link between longitudinal tau accumulation and iFC to tau epicenters [48]. Moreover, our study builds upon these studies by looking on a voxel-by-voxel basis at both topographical overlap and correlation between iFC and tau. Furthermore, our work complements studies showing that FCNs related to pathological tau-peaks have increased tau load and resemble healthy rs-FCNs. Our study focuses the iFC analysis on specific Braak stages, revealing correlations that link the Braak stages with successive tau-peaks and levels of functional connectivity.

Stepwise tau topographical overlap and correlation through Braak stages

By comparing how the overall distribution of tau fits within FCNs, as well as voxel-by-voxel correlations between iFC and tau, we demonstrate a topographical and correlational relationship between the network degeneration hypothesis and Braak stages. We believe that these results are consistent with the concept that tau pathology progresses along specific intra-neuronal connectivity pathways defined either by structural connectivity, by pathways defined by areas that are strongly functionally connected, or both.

Directionality of hypothesized tau progression

We found overlap of spatial topography and significant correlations between tau-peak iFC (in HC) and tau deposition (AD > HC) within Braak stages both more and less advanced than the location of tau-peaks. In the Braak staging model, tau is proposed to flow successively, in an anterograde pattern, from the entorhinal cortex through to higher cortical areas. However, several studies have additionally suggested a retrograde progression of tau pathology [13–15].

Although a relationship between tau deposition levels and iFC could be expected in unidirectional functionally based tau progression, these relationships also suggest the bidirectional progression of tau, without providing proof thereof. Importantly, iFC levels were computed in HC subjects to avoid the network disruptions caused by tau and Aβ [39, 42, 55]. First, there were significant correlations between voxel-

wise tau levels and iFC to tau-peaks in those same voxels. Second, iFC was specific for tau pathology in distant ROIs, based on the GOF analysis and *t* tests. These relationships could be interpreted that tau flows from a tau-peak into the peak's functionally connected voxels; however, it is more logical that tau converges on the tau-peaks, making them relative maximums of tau pathology. We believe that it is implicit that tau follows pathways of healthy functional connectivity rather than the converse, which would imply that iFC in healthy subjects is somehow impacted by the extent of pathological tau deposition in AD subjects. Under the hypothesis that tau progresses unidirectionally, there could also be a correlation between tau and iFC. Bidirectional progression of tau pathology, however, is suggested as the GOF, coupled with a positive correlation between iFC and tau levels, indicates that iFC was not only directly related to the voxel-wise extent of tau, but it was also topographically specific for tau. So, while the positive correlations between iFC and tau do not imply causality of the direction in which tau progresses, they are consistent with tau's progression through functional relationships, utilizing tau-peaks as highly connected hubs in the process.

Limitations

First, we did not correct for multiple comparisons when defining the distribution of tau used in our *t* tests or correlation analysis. We believe that this is acceptable for two reasons. (1) Our visual distribution of tau uptake strongly resembled that of other published studies [17, 18, 34]. (2) Our *t* tests and correlation analysis captured more generally the relative extent of AD > HC tau deposition, making the FWE correction arguably too conservative by eliminating many voxels.

Next, the chronology of tau progression suggested in this study remains speculative. Data was examined in a cross-sectional, groupwise manner, which does not provide proof for a longitudinal progression of tau pathology in individual patients. Additionally, AD patients at different stages of disease were not included in this study. Therefore, while our results are consistent with regional tau pathology correlating with functional connectivity relationships, they do not provide evidence that tau progresses or expands within those relationships. Additionally, there is emerging evidence that the pattern of tau progression might be more variable than can be accounted for by the Braak stages, with multiple identified phenotypes of tau progression [54], which was not explored in this study. Finally, we believe that GOF scores, such as those used in our analysis, might be better suited in longitudinal studies to better account for individual or phenotypic variation in tau-PET levels.

Next, iFC may be prone to a nearness effect, whereby voxels close to the tau-peak have a higher iFC value. Euclidean distance was used to attempt to control for this bias; however, it introduced a new systematic bias. Some tau-iFC correlations became unexpectedly stronger due to a strong negative correlation between tau and Euclidean distance in certain regions. Thus, we excluded a sphere of 10 mm around the 4-mm sphere used to define each tau-peak to eliminate the region most prone to this bias.

Finally, our FC analyses utilized a group of HC subjects much younger than the tau-tracer imaging subjects (see Table 1). This dataset of fMRI scans was previously utilized [26] and was chosen to identify typical networks not influenced by neurodegenerative pathology [19, 56]. Nevertheless, aging and AD progression could have altered various FCNs [5], weakening the correspondence between FCNs and tau deposition in Braak stages observed in our study.

Future directions

Network diffusion models have been shown to predict the pattern of tau progression [57], and these models could be implemented to model the spatial distribution of tau within Braak stages. Longitudinal data could also be incorporated, to test for stepwise and chronological changes in tau pathology, especially across stages of Alzheimer's disease. Finally, our study measured iFC within HC; however, future studies could capture network activity directly in patients to more directly determine tau's effect on connectivity.

Conclusion

Our study is original in that it is the first to establish a stepwise link between tau deposition and functional connectivity through the Braak stages in AD subjects. These findings help account for tau pathology in multiple large-scale functional networks, as reported in previous studies. These results show that the connectivity of each region affected by tau pathology could account for future progression into more advanced Braak stages and intensification of tau pathology in less advanced Braak stages, although additional study is warranted to isolate this pattern in other proposed subtypes of tau pathology progression. Our study is the first study to find both voxel-wise topographical overlap and a voxel-wise positive correlation between iFC and tau. Our results are consistent with the neuropathological Braak stage model of tau deposition and support the NDH. This study is further original in suggesting an upstream and downstream theory of tau pathology progression, where tau-peaks are related to further accumulation in both anterograde and retrograde directions within the Braak stages.

Acknowledgments We thank all the patients who participated in this study as well as their friends and family, and the staff at the University Hospital of Cologne Department of Nuclear Medicine. We thank Michael Greicius, M.D., Ph.D., and Mojtaba Zarei, M.D., Ph.D., for their helpful comments. Data used in preparation of this article were obtained from the Alzheimer's Disease Neuroimaging Initiative (ADNI) database (adni.loni.usc.edu). As such, the investigators within the ADNI contributed to the design and implementation of ADNI and/or provided data but did not participate in analysis or writing of this report. A complete listing of ADNI investigators can be found at: http://adni.loni.usc.edu/wp-content/uploads/how_to_apply/ADNI_Acknowledgement_List.pdf

Author contributions A.D., G.B., and J.S. conceived the project. All authors designed and executed the experiments to analyze the data and interpret the results. J.S., G.B., and A.D. wrote the manuscript. All authors edited the manuscript.

Funding This project was supported by funding from the DFG (German Research Foundation) DR 445/9-1 to A.D. and T.v.E., a Fulbright Program grant to J.S. sponsored by the Bureau of Educational and Cultural Affairs of the United States Department of State and administered by the Institute of International Education. Data collection and sharing for this project was funded by the Alzheimer's Disease Neuroimaging Initiative (ADNI) (National Institutes of Health Grant U01 AG024904) and DOD ADNI (Department of Defense award number W81XWH-12-2-0012). ADNI is funded by the National Institute on Aging, the National Institute of Biomedical Imaging and Bioengineering, and through generous contributions from the following: AbbVie, Alzheimer's Association; Alzheimer's Drug Discovery Foundation; Araclon Biotech; BioClinica, Inc.; Biogen; Bristol-Myers Squibb Company; CereSpir, Inc.; Cogstate; Eisai Inc.; Elan Pharmaceuticals, Inc.; Eli Lilly and Company; EuroImmun; F. Hoffmann-La Roche Ltd. and its affiliated company Genentech, Inc.; Fujirebio; GE Healthcare; IXICO Ltd.; Janssen Alzheimer Immunotherapy Research & Development, LLC.; Johnson & Johnson Pharmaceutical Research & Development LLC.; Lumosity; Lundbeck; Merck & Co., Inc.; Meso Scale Diagnostics, LLC.; NeuroRx Research; Neurotrack Technologies; Novartis Pharmaceuticals Corporation; Pfizer Inc.; Piramal Imaging; Servier; Takeda Pharmaceutical Company; and Transition Therapeutics. The Canadian Institutes of Health Research is providing funds to support ADNI clinical sites in Canada. Private sector contributions are facilitated by the Foundation for the National Institutes of Health (www.fnih.org). The grantee organization is the Northern California Institute for Research and Education, and the study is coordinated by the Alzheimer's Therapeutic Research Institute at the University of Southern California. ADNI data are disseminated by the Laboratory for Neuro Imaging at the University of Southern California.

Compliance with ethical standards

This article does not contain any studies with human participants or animals performed by any of the authors; all imaging data was obtained through independent repositories as described in methods.

Conflict of interest The authors declare that they have no conflict of interest.

References

1. Seeley WW, Carlin DA, Allman JM, Macedo MN, Bush C, Miller BL, et al. Early frontotemporal dementia targets neurons unique to apes and humans. Ann Neurol. 2006;60:660–7.
2. Seeley WW. Selective functional, regional, and neuronal vulnerability in frontotemporal dementia. Curr Opin Neurol. 2008;21:701–7.
3. Buckner RL. Molecular, structural, and functional characterization of Alzheimer's disease: evidence for a relationship between default activity, amyloid, and memory. J Neurosci. 2005;25:7709–17.
4. Franzmeier N, Rubinski A, Neitzel J, Kim Y, Damm A, Na DL, et al. Functional connectivity associated with tau levels in ageing, Alzheimer's, and small vessel disease. Brain. 2019;142:1093–107.
5. Seeley WW, Crawford RK, Zhou J, Miller BL, Greicius MD. Neurodegenerative diseases target large-scale human brain networks. Neuron. 2009;62:42–52.
6. Tahmasian M, Shao J, Meng C, Grimmer T, Diehl-Schmid J, Yousefi BH, et al. Based on the network degeneration hypothesis: separating individual patients with different neurodegenerative syndromes in a preliminary hybrid PET/MR study. J Nucl Med. 2016;57:410–5.
7. Tahmasian M, Pasquini L, Scherr M, Meng C, Förster S, Mulej Bratec S, et al. The lower hippocampus global connectivity, the higher its local metabolism in Alzheimer disease. Neurology. 2015;84:1956–63.
8. Hansson O, Grothe MJ, Strandberg TO, Ohlsson T, Hägerström D, Jögi J, et al. Tau pathology distribution in Alzheimer's disease corresponds differentially to cognition-relevant functional brain networks. Front Neurosci. 2017;11:167.
9. Cope TE, Rittman T, Borchert RJ, Jones PS, Vatansever D, Allinson K, et al. Tau burden and the functional connectome in Alzheimer's disease and progressive supranuclear palsy. Brain. 2018;141:550–67.
10. Hoenig MC, Bischof GN, Seemiller J, Hammes J, Kukolja J, Onur ÖA, et al. Networks of tau distribution in Alzheimer's disease. Brain. 2018;2:568–81.
11. Jones DT, Graff-Radford J, Lowe VJ, Wiste HJ, Gunter JL, Senjem ML, et al. Tau, amyloid, and cascading network failure across the Alzheimer's disease spectrum. Cortex. 2017;97:143–59.
12. Braak H, Braak E. Neuropathological stageing of Alzheimer-related changes. Acta Neuropathologica. 1991;82:239–59.
13. Wu JW, Herman M, Liu L, Simoes S, Acker CM, Figueroa H, et al. Small misfolded tau species are internalized via bulk endocytosis and anterogradely and retrogradely transported in neurons. J Biol Chem. 2013;288:1856–70.
14. Ahmed Z, Cooper J, Murray TK, Garn K, McNaughton E, Clarke H, et al. A novel in vivo model of tau propagation with rapid and progressive neurofibrillary tangle pathology: the pattern of spread is determined by connectivity, not proximity. Acta Neuropathologica. 2014;127:667–83.
15. Sanders DW, Kaufman SK, DeVos SL, Sharma AM, Mirbaha H, Li A, et al. Distinct tau prion strains propagate in cells and mice and define different tauopathies. Neuron. 2014;82:1271–88.
16. Zempel H, Thies E, Mandelkow E, Mandelkow E-M. A Oligomers cause localized Ca2+ elevation, missorting of endogenous tau into dendrites, tau phosphorylation, and destruction of microtubules and spines. J Neurosci. 2010;30:11938–50.
17. Cho H, Choi JY, Hwang MS, Kim YJ, Lee HM, Lee HS, et al. In vivo cortical spreading pattern of tau and amyloid in the Alzheimer disease spectrum: tau and amyloid in AD. Ann Neurol. 2016;80:247–58.
18. Schwarz AJ, Yu P, Miller BB, Shcherbinin S, Dickson J, Navitsky M, et al. Regional profiles of the candidate tau PET ligand ^{18}F-AV-1451 recapitulate key features of Braak histopathological stages. Brain. 2016;139:1539–50.
19. Schöll M, Lockhart SN, Schonhaut DR, O'Neil JP, Janabi M, Ossenkoppele R, et al. PET imaging of tau deposition in the aging human brain. Neuron. 2016;89:971–82.
20. Jack CR, Bernstein MA, Fox NC, Thompson P, Alexander G, Harvey D, et al. The Alzheimer's disease neuroimaging initiative (ADNI): MRI methods. J Magn Reson Imaging. 2008;27:685–91.

21. Gonzalez-Escamilla G, Lange C, Teipel S, Buchert R, Grothe MJ. PETPVE12: an SPM toolbox for partial volume effects correction in brain PET–application to amyloid imaging with AV45-PET. NeuroImage. 2017;147:669–77.
22. Diedrichsen J. A spatially unbiased atlas template of the human cerebellum. NeuroImage. 2006;33:127–38.
23. Baker SL, Maass A, Jagust WJ. Considerations and code for partial volume correcting [18F]-AV-1451 tau PET data. Data Brief. 2017;15:648–57.
24. Amunts K, Kedo O, Kindler M, Pieperhoff P, Mohlberg H, Shah NJ, et al. Cytoarchitectonic mapping of the human amygdala, hippocampal region and entorhinal cortex: intersubject variability and probability maps. Anat Embryol (Berl). 2005;210:343–52.
25. Hoenig MC, Bischof GN, Hammes J, Faber J, Fliessbach K, van Eimeren T, et al. Tau pathology and cognitive reserve in Alzheimer's disease. Neurobiol Aging. 2017;57:1–7.
26. Biswal BB, Mennes M, Zuo X-N, Gohel S, Kelly C, Smith SM, et al. Toward discovery science of human brain function. Proc Natl Acad Sci. 2010;107:4734–9.
27. Yan. DPARSF: a MATLAB toolbox for "pipeline" data analysis of resting-state fMRI. Front Syst Neurosci. 2010;4:13
28. Power JD, Mitra A, Laumann TO, Snyder AZ, Schlaggar BL, Petersen SE. Methods to detect, characterize, and remove motion artifact in resting state fMRI. NeuroImage. 2014;84:320–41.
29. Murphy K, Birn RM, Handwerker DA, Jones TB, Bandettini PA. The impact of global signal regression on resting state correlations: are anti-correlated networks introduced? NeuroImage. 2009;44:893–905.
30. Chai XJ, Castañón AN, Öngür D, Whitfield-Gabrieli S. Anticorrelations in resting state networks without global signal regression. NeuroImage. 2012;59:1420–8.
31. Fox MD, Zhang D, Snyder AZ, Raichle ME. The global signal and observed anticorrelated resting state brain networks. J Neurophysiol. 2009;101:3270–83.
32. Friston KJ, Williams S, Howard R, Frackowiak RSJ, Turner R. Movement-related effects in fMRI time-series. Magn Reson Med. 1996;35:346–55.
33. Diedenhofen B, Musch J. cocor: A Comprehensive solution for the statistical comparison of correlations. PLoS One. 2015;10: e0121945.
34. Chien D, Shadfar B, Katrin SA, C WJ, Fanrong M, Min-Ying S, et al. Early clinical PET imaging results with the novel PHF-tau radioligand [F-18]-T807. J Alzheimeraposs Dis. 2013;38:171–84.
35. Vermersch P, Frigard B, David J-P, Fallet-Bianco C, Delacourte A. Presence of abnormally phosphorylated Tau proteins in the entorhinal cortex of aged non-demented subjects. Neurosci Lett. 1992;144:143–6.
36. Yang W, Ang LC, Strong MJ. Tau protein aggregation in the frontal and entorhinal cortices as a function of aging. Dev Brain Res. 2005;156:127–38.
37. Vermersch P, David J-P, Frigard B, Fallet-Bianco C, Wattez A, Petit H, et al. Cortical mapping of Alzheimer pathology in brains of aged non-demented subjects. Prog Neuro-Psychopharmacol Biol Psychiatry. 1995;19:1035–47.
38. Buckner RL, Sepulcre J, Talukdar T, Krienen FM, Liu H, Hedden T, et al. Cortical hubs revealed by intrinsic functional connectivity: mapping, assessment of stability, and relation to Alzheimer's disease. J Neurosci. 2009;29:1860–73.
39. Braak H, Del Tredici K. Alzheimer's pathogenesis: is there neuron-to-neuron propagation? Acta Neuropathol (Berl). 2011;121:589–95.
40. Prusiner SB. Some speculations about prions, amyloid, and Alzheimer's disease. N Engl J Med. 1984;310:661–3.
41. Zhou J, Gennatas ED, Kramer JH, Miller BL, Seeley WW. Predicting regional neurodegeneration from the healthy brain functional connectome. Neuron. 2012;73:1216–27.
42. Raj A, Kuceyeski A, Weiner M. A network diffusion model of disease progression in dementia. Neuron. 2012;73:1204–15.
43. Saxena S, Caroni P. Selective neuronal vulnerability in neurodegenerative diseases: from stressor thresholds to degeneration. Neuron. 2011;71:35–48.
44. de Haan W, Mott K, van Straaten ECW, Scheltens P, Stam CJ. Activity dependent degeneration explains hub vulnerability in Alzheimer's disease. Sporns O, editor. PLoS Comput Biol. 2012;e1002582:8.
45. Appel SH. A unifying hypothesis for the cause of amyotrophic lateral sclerosis, parkinsonism, and alzheimer disease. Ann Neurol. 1981;10:499–505.
46. Iba M, Guo JL, McBride JD, Zhang B, Trojanowski JQ, Lee VM-Y. Synthetic tau fibrils mediate transmission of neurofibrillary tangles in a transgenic mouse model of Alzheimer's-like tauopathy. J Neurosci. 2013;33:1024–37.
47. Stancu I-C, Vasconcelos B, Ris L, Wang P, Villers A, Peeraer E, et al. Templated misfolding of tau by prion-like seeding along neuronal connections impairs neuronal network function and associated behavioral outcomes in tau transgenic mice. Acta Neuropathol (Berl). 2015;129:875–94.
48. Franzmeier N, Dewenter A, Frontzkowski L, Dichgans M, Rubinski A, Neitzel J, et al. Patient-centered connectivity-based prediction of tau pathology spread in Alzheimer's disease. Sci Adv. 2020;6:eabd1327.
49. Vogel JW, Mattsson N, Iturria-Medina Y, Strandberg OT, Schöll M, Dansereau C, et al. Data-driven approaches for tau-PET imaging biomarkers in Alzheimer's disease. Hum Brain Mapp. 2019;40:638–51.
50. Ossenkoppele R, Schonhaut DR, Schöll M, Lockhart SN, Ayakta N, Baker SL, et al. Tau PET patterns mirror clinical and neuroanatomical variability in Alzheimer's disease. Brain. 2016;139:1551–67.
51. Murray ME, Graff-Radford NR, Ross OA, Petersen RC, Duara R, Dickson DW. Neuropathologically defined subtypes of Alzheimer's disease with distinct clinical characteristics: a retrospective study. Lancet Neurol. 2011;10:785–96.
52. Ossenkoppele R, Lyoo CH, Sudre CH, Westen D, Cho H, Ryu YH, et al. Distinct tau PET patterns in atrophy-defined subtypes of Alzheimer's disease. Alzheimers Dement. 2020;16:335–44.
53. Day GS, Gordon BA, Jackson K, Christensen JJ, Rosana Ponisio M, Su Y, et al. Tau-PET binding distinguishes patients with early-stage posterior cortical atrophy from amnestic Alzheimer disease dementia. Alzheimer Dis Assoc Disord. 2017;31:87–93.
54. Vogel JW, Young AL, Oxtoby NP, Smith R, Ossenkoppele R, Strandberg OT, et al. Characterizing the spatiotemporal variability of Alzheimer's disease pathology. medRxiv. 2020.
55. Palop JJ, Mucke L. Amyloid-β–induced neuronal dysfunction in Alzheimer's disease: from synapses toward neural networks. Nat Neurosci. 2010;13:812–8.
56. Villemagne VL, Ong K, Mulligan RS, Holl G, Pejoska S, Jones G, et al. Amyloid imaging with 18F-Florbetaben in Alzheimer disease and other dementias. J Nucl Med. 2011;52:1210–7.
57. Vogel JW, Iturria-Medina Y, Strandberg OT, Smith R, Levitis E, Evans AC, et al. Spread of pathological tau proteins through communicating neurons in human Alzheimer's disease. Nat Commun. 2020;11:2612.